Romanian Reports in Physics, Vol. 65, No. 4, P. 1301–1313, 2013

Sn ISOTOPES: A STUDY WITHIN RMF+BCS APPROACH

G. SAXENA[1], D. SINGH[2], M. KAUSHIK[3]

[1]Department of Physics, Govt. Women Engineering College, Ajmer-305002, India
E-mail: gauravphy@gmail.com
[2]Department of Physics, University of Rajasthan, Jaipur-302004, India
[3]Department of Physics, Shankara Institute of Technology, Jaipur-302028, India

Received December 9, 2012

Abstract. Inspired by recent experimental activities on Sn isotopes we have employed Relativistic Mean Field (RMF) plus BCS approach to study the ground state properties of entire chain of Sn isotopes from proton drip line to neutron drip line. We have analysed separation energy, deformations, the role of single particle states lying close to the Fermi surface, rms radii and the related density profiles etc. to elucidate our findings. For neutron rich isotopes role of resonant states and skin formation is described in detail. Our results of rms radii and separation energy are in excellent agreement with experimental data.

Key words: Relativistic Mean Field, Drip Line Nuclei, Sn Isotopes, Neutron Skin.

1. INTRODUCTION

With ever increasing technological progress in acceleration and detection facilities, we have now the possibility of having access to about 8000 distinct radioactive nuclei which live long enough to be candidates for acceleration. This possibility should enable us to probe the limits of existence of nuclei with large difference in N and Z values [1, 2]. The majority of experimental investigations of exotic nuclei, as mentioned above, have rather been related to the neutron rich cases in the lighter mass region. These neutron rich nuclei away from the line of β-stability with unusually large isospin value exhibit several interesting features. For example, nuclei close to the neutron drip-line show a much extended tail for the neutron density distribution and have a diffused neutron skin while the Fermi level lies close to the single particle continuum. In some cases it may even lead to the phenomenon of neutron halo, as observed experimentally in the case of light nuclei [1, 2].

Theoretical studies of neutron and proton rich nuclei away from the valley of β-stability have been mostly carried out within the framework of mean-field theories [3]-[9], and also employing their relativistic counterparts [10] - [26]. Earlier the effect of continuum on the pairing energy contribution has been calculated by Grasso *et al*. [7] and Sandulescu *et al*. [8] within the HF+BCS+Resonant continuum approach. Similarly the effect of inclusion of positive energy resonant states on the pairing cor-

relations has been investigated for the unstable nuclei by Yadav *et al.* [22] within the framework of relativistic mean-field (RMF) theory. The interesting result of these studies is that only a few low energy resonant states, especially those near the Fermi surface influence in an appreciable way the pairing properties of neutron rich isotopes of some nuclei far from the line of β-stability. This finding is of immense significance because one can eventually make use of this for systematic studies of a large number of nuclei by employing a simpler HF+BCS or alternatively the RMF+BCS approximation. Indeed the RMF+BCS scheme [22] yields results which are in close agreement with the experimental data and with those of recent continuum relativistic Hartree-Bogoliubov (RCHB) and other similar mean-field calculations [23, 27].

Recently the Sn isotopes have drawn much attention due to its two doubly magic isotopes, the proton rich ^{100}Sn and the neutron rich ^{132}Sn, both of which have been produced experimentally [28, 29]. More recently measurements of the half-life and decay energy for the decay of ^{100}Sn is reported by Hinke *et al*. [30]. These findings have motivated us to investigate the Sn isotopes in rather detailed manner throughout from its proton to neutron drip-lines within the RMF+BCS approach.

In the present investigations, the RMF calculations for Sn isotopes studied here have been carried out assuming a symmetrically deformed shape and have been referred to throughout as deformed RMF calculations. Our extensive calculations, though most of them not shown here, reveal that majority of isotopes for the proton magic numbers have spherical or almost close to a spherical shape with a negligible deformation. This situation has been beneficially utilized as explained in the following. Since description of spherical nuclei becomes easier and transparent in terms of spherical single particle wave functions and energies, we have preferred to analyse and discuss the results of these nuclei with negligible deformation within the framework of a spherical RMF+BCS description (referred to throughout as spherical RMF approach) for convenience. This is especially true for the understanding of shell closures and magicity, and also for the behaviour of single particle states near the Fermi surface which in turn plays an important role near the drip-line. Similarly, within such a spherical framework contributions of neutron and proton single particle states to the density profiles, pairing gaps, total pairing energy etc. which are also equally important in the study of exotic phenomena can be demonstrated with clarity. These aspects of the spherical RMF+BCS framework indeed make this approach very useful, especially for the study of poorly understood exotic nuclei. Thus, in our presentation we have utilized this advantage while discussing the results of nuclei which are found to be spherical in shape. For our calculations in both approaches, the deformed RMF and the spherical RMF, we have employed the TMA [16] Lagrangian density, extensively used in the relativistic mean-field calculations [22, 26, 31].

2. RELATIVISTIC MEAN FIELD PLUS BCS APPROACH

Our RMF calculations have been carried out using the model Lagrangian density with nonlinear terms both for the σ and ω mesons along with the TMA parametrization as described in detail in Refs. [16, 22, 25].

$$\begin{aligned}\mathcal{L} = \bar{\psi}[\imath\gamma^{\mu}\partial_{\mu} - M]\psi + \frac{1}{2}\partial_{\mu}\sigma\partial^{\mu}\sigma - \frac{1}{2}m_{\sigma}^{2}\sigma^{2} - \frac{1}{3}g_{2}\sigma^{3} - \frac{1}{4}g_{3}\sigma^{4} - g_{\sigma}\bar{\psi}\sigma\psi \\ - \frac{1}{4}H_{\mu\nu}H^{\mu\nu} + \frac{1}{2}m_{\omega}^{2}\omega_{\mu}\omega^{\mu} + \frac{1}{4}c_{3}(\omega_{\mu}\omega^{\mu})^{2} - g_{\omega}\bar{\psi}\gamma^{\mu}\psi\omega_{\mu} \\ - \frac{1}{4}G_{\mu\nu}^{a}G^{a\mu\nu} + \frac{1}{2}m_{\rho}^{2}\rho_{\mu}^{a}\rho^{a\mu} - g_{\rho}\bar{\psi}\gamma_{\mu}\tau^{a}\psi\rho^{\mu a} \\ - \frac{1}{4}F_{\mu\nu}F^{\mu\nu} - e\bar{\psi}\gamma_{\mu}\frac{(1-\tau_{3})}{2}A^{\mu}\psi, \quad (1)\end{aligned}$$

where the field tensors H, G and F for the vector fields are defined by

$$\begin{aligned}H_{\mu\nu} &= \partial_{\mu}\omega_{\nu} - \partial_{\nu}\omega_{\mu} \\ G_{\mu\nu}^{a} &= \partial_{\mu}\rho_{\nu}^{a} - \partial_{\nu}\rho_{\mu}^{a} - 2g_{\rho}\,\epsilon^{abc}\rho_{\mu}^{b}\rho_{\nu}^{c} \\ F_{\mu\nu} &= \partial_{\mu}A_{\nu} - \partial_{\nu}A_{\mu},\end{aligned}$$

and other symbols have their usual meaning. Based on the single-particle spectrum calculated by the RMF described above, we perform a state dependent BCS calculations[32, 33]. As we already mentioned, the continuum is replaced by a set of positive energy states generated by enclosing the nucleus in a spherical box. Thus the gap equations have the standard form for all the single particle states, *i.e.*

$$\Delta_{j_1} = -\frac{1}{2}\frac{1}{\sqrt{2j_1+1}}\sum_{j_2}\frac{\left\langle (j_1{}^2)\,0^{+}\,|V|\,(j_2{}^2)\,0^{+}\right\rangle}{\sqrt{\left(\varepsilon_{j_2}-\lambda\right)^{2}+\Delta_{j_2}^{2}}}\,\sqrt{2j_2+1}\;\Delta_{j_2}\;, \qquad (2)$$

where ε_{j_2} are the single particle energies, and λ is the Fermi energy, whereas the particle number condition is given by $\sum_j (2j+1)v_j^2 = \mathrm{N}$. In the calculations we use for the pairing interaction a delta force, *i.e.*, V = -$\mathrm{V}_0\delta(r)$ with the same strength V_0 for both protons and neutrons. The value of the interaction strength V_0 = 350 MeV fm^3 was determined in ref.[22] by obtaining a best fit to the binding energy of Ni isotopes. We use the same value of V_0 for our present studies of isotopes of other nuclei as well. Apart from its simplicity, the applicability and justification of using such a δ-function form of interaction has been recently discussed in Refs.[3], whereby it has been shown in the context of HFB calculations that the use of a delta force in a finite space simulates the effect of finite range interaction in a phenomenological manner (see also[34] and[35] for more details). The pairing matrix element for the

δ-function force is given by

$$\left\langle (j_1{}^2)\,0^+\,|V|\,(j_2{}^2)\,0^+\right\rangle = -\frac{V_0}{8\pi}\sqrt{(2j_1+1)(2j_2+1)}\,I_R\,, \tag{3}$$

where I_R is the radial integral having the form

$$I_R = \int dr \frac{1}{r^2}\left(G^\star_{j_1}\,G_{j_2} + F^\star_{j_1}\,F_{j_2}\right)^2 \tag{4}$$

Here G_α and F_α denote the radial wave functions for the upper and lower components, respectively, of the nucleon wave function expressed as

$$\psi_\alpha = \frac{1}{r}\begin{pmatrix} i\;G_\alpha\;\mathcal{Y}_{j_\alpha l_\alpha m_\alpha} \\ F_\alpha\,\sigma\cdot\hat{r}\;\mathcal{Y}_{j_\alpha l_\alpha m_\alpha}\end{pmatrix}\,, \tag{5}$$

and satisfy the normalization condition

$$\int dr\,\{|G_\alpha|^2 + |F_\alpha|^2\} = 1 \tag{6}$$

In Eq. (5) the symbol $\mathcal{Y}_{jlm}$ has been used for the standard spinor spherical harmonics with the phase i^l. The coupled field equations obtained from the Lagrangian density in (1) are finally reduced to a set of simple radial equations [13] which are solved self consistently along with the equations for the state dependent pairing gap Δ_j and the total particle number N for a given nucleus.

The relativistic mean field description has been extended for the deformed nuclei of axially symmetric shapes by Gambhir, Ring and their collaborators [14] using an expansion method. The treatment of pairing has been carried out in Ref. [31] using state dependent BCS method [32] as has been given by Yadav *et al.* [22] for the spherical case. For axially deformed nuclei the rotational symmetry is no more valid and the total angular momentum j is no longer a good quantum number. Nevertheless, the various densities still are invariant with respect to a rotation around the symmetry axis. Here we have taken the symmetry axis to be the z-axis. Following Gambhir *et al.* [14], it is then convenient to employ the cylindrical coordinates.

The scalar, vector, isovector and charge densities, as in the spherical case, are expressed in terms of the spinor π_i, its conjugate π_i^+, operator τ_3 etc. These densities serve as sources for the fields ϕ = σ, ω^0 ρ^0 and A^0, which are determined by the Klein-Gordon equation in cylindrical coordinates. Thus a set of coupled equations, namely the Dirac equation with potential terms for the nucleons and the Klein-Gordon type equations with sources for the mesons and the photon is obtained. These equations are solved self consistently. For this purpose, as described above, the well-tested basis expansion method has been employed [14]. The bases used here are generated by an anisotropic (axially symmetric) harmonic oscillator potential. The upper and lower components of the nucleon spinors, the fields as well as the baryon currents and densities, are expanded separately in these bases. The expansion is trun-

cated so as to include all the configurations up to a certain finite value of the major oscillator shell quantum number. In this expansion method the solution of the Dirac equation gets reduced to a symmetric matrix diagonalising problem, while that of the Klein-Gordon equation reduces to a set of inhomogeneous equations. The solution provides the spinor fields, and the nucleon currents and densities (sources of the fields), from which all the relevant ground state nuclear properties are calculated. For further details of these formulations we refer the reader to ref. [14, 31].

3. RESULTS AND DISCUSSION

In order to identify the two neutron and two proton drip-lines for the Sn isotopes we have displayed in Figs. 1 and 2, respectively, the variation of two neutron separation energy S_{2n}, and that of two proton separation energy S_{2p} with increasing neutron number N.

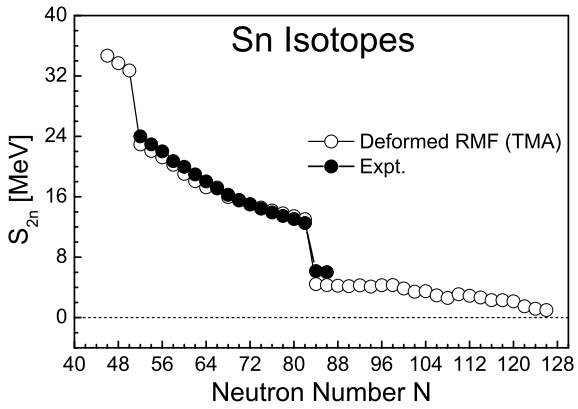

Fig. 1 – Calculated results for the two neutron separation energy obtained within the deformed RMF approach for the $^{98-176}$Sn isotopes. These results have been compared with the available experimental data [36] for the isotopes $^{104-136}$Sn.

It is gratifying to note that the two neutron and two proton separation energy values obtained in the deformed RMF approach are in reasonably good agreement with the available experimental data [36]. It is clearly evident from the Fig. 1 that the two neutron drip-line for the Sn isotopic chain occurs at the neutron number N = 126, a traditional neutron magic number. Thus, nucleus ^{176}Sn is found to be the heaviest bound isotope of Sn. Similarly our calculations show that the two proton drip-line for Sn isotopes occurs at the neutron number N = 46 which correspond to A = 96 as can be seen from Fig. 2. The two neutron separation energy shows a distinctive

signature at the neutron shell closures. Thus a close inspection of Fig. 1 shows rapid decrease in the S_{2n} value at the neutron numbers N = 50 and 82 corresponding to the neutron shell closures. These neutron shell closures as revealed by the two neutron separation energy plot can also be confirmed by the total pairing energy obtained in the spherical RMF approach for the Sn isotopes.

It is found that the contribution to the total pairing energy is mostly from the neutron single particle states. Thus for the proton magic nuclei, the total pairing energy vanishes for the N values corresponding to the neutron shell closures as these correspond to doubly magic nuclei. It is found that the pairing energy vanishes for $N = 50$ and $N = 82$ due to shell closure. The pairing energy values obtained in the spherical RMF approach are found to be of similar magnitude as those obtained in other mean-field calculations [5, 9, 20].

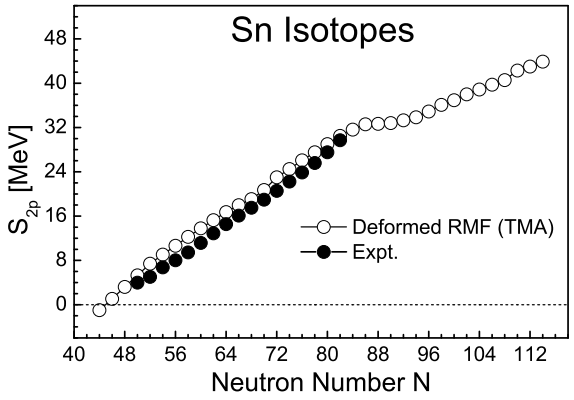

Fig. 2 – Calculated results for the two proton separation energy obtained within the deformed RMF approach for the $^{94-172}$Sn isotopes. These results have been compared with the available experimental data [36] for the isotopes $^{102-136}$Sn.

From the above remarks it is evident that the chain of the bound isotopes of Sn is very long (from A = 96 to A = 176) and the lightest isotope of Sn is found ^{96}Sn, around which a region near proton drip line can be explored in future experimental studies as measurements of ^{100}Sn has recently been reported by Hinke *et al.* [30]. We have also investigated nucleus ^{94}Sn which is beyond proton drip line. It is found that this nucleus has one proton separation energy S_p = 0.014 MeV and two proton separation energy S_{2p} = -0.976 MeV. In context to recent studies on two proton radioactivity [25] this nucleus ^{94}Sn satisfying the criteria $S_p > 0$ and $S_{2p} < 0$ and may be a possible candidate of two proton radioactivity.

On the other side the isotope as heavy as ^{176}Sn is found to be bound with

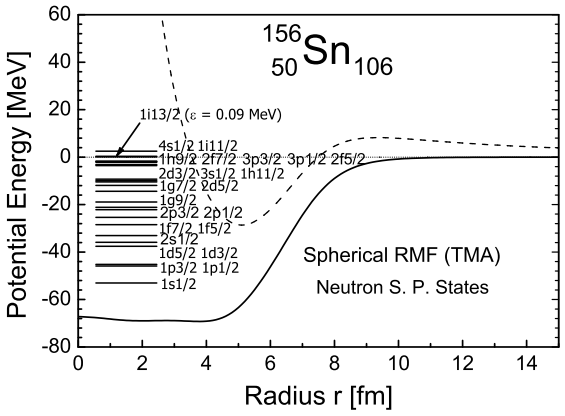

Fig. 3 – The potential energy plot (sum of the scalar and vector potentials), for the neutron rich isotope ^{156}Sn as a function of radius. Besides the position of resonant state $1i_{13/2}$, the plot also shows the energy spectrum of the bound neutron single particle states. The long dashed line represents the sum of RMF potential energy and the centrifugal barrier energy for the neutron resonant state $1i_{13/2}$. These results have been obtained within the spherical RMF approach.

neutron to proton ratio of 2.52. Interestingly, the deformed RMF calculations further show that almost all the Sn isotopes have the spherical shape as the values of quadrupole deformation parameter is zero for all isotopes. This situation is utilized to our advantage by carrying out our detailed study of the Sn isotopes, especially the exotic ones lying close to the proton and neutron drip-lines within the framework of spherical RMF approach as has been done earlier for the nuclei with zero or near zero deformation.

For such a detailed investigation, we have chosen the neutron rich nucleus ^{156}Sn as the representative example of Sn isotopes located in the vicinity of the neutron drip-line. This has been done in order to elucidate the important results for the RMF potential, the spherical single particle wave functions and the single particle energies, the pairing gap energy, proton and neutron density profiles and the rms radii for the proton and neutron distributions etc. In Fig. 3 we have displayed the RMF potential, a sum of scalar and vector potentials, for the nucleus ^{156}Sn along with the spectrum for the bound neutron single particle states. The plot also depicts some positive energy single particle states near the Fermi level, besides the resonant state $1i_{13/2}$ located at 0.09 MeV which play important role in the contribution to the total pairing energy. For the $1i_{13/2}$ resonant state we have also shown by long dashed lines the total mean-field potential given by a sum of RMF potential energy and the centrifugal barrier energy. It is evident from the plot that the effective total potential for the resonant state $1i_{13/2}$ in ^{156}Sn has an appreciable barrier for the confinement

of waves to form a quasi-bound or resonant state.

The wave function of this state exhibits characteristics similar to that of a bound state as is seen in Fig. 4.

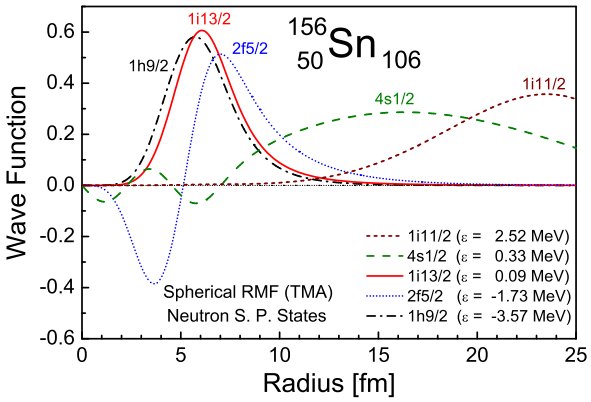

Fig. 4 – Radial wave functions of a few representative neutron single particle states with energy close to the Fermi surface obtained within the spherical RMF approach for the neutron rich nucleus ^{156}Sn. The low lying neutron resonant state $1i_{13/2}$ has been depicted by the solid line. The resonant state similar to the bound states is mostly confined within the potential region. In contrast, the other non-resonant continuum states, for example, $4s_{1/2}$ and $1i_{11/2}$ have their major part of the wave function spread over outside the potential region.

In contrast, the main part of the wave functions for the non-resonant states for the neutron rich nuclei is seen to be mostly spread over outside their potential region. The wave function of the neutron single particle states $4s_{1/2}$ and $1i_{11/2}$ in ^{156}Sn displayed in Fig. 4 represent typical examples of such states.

For this nucleus the $1i_{13/2}$ state lies at ϵ = 0.09 MeV, whereas the Fermi energy is seen to be at ϵ_f = -1.76 MeV. Some of the important neutron single particle states near the Fermi surface for the neutron rich nucleus ^{156}Sn include the positive energy states $4s_{1/2}$ at ϵ = 0.33 MeV, the resonant state $1i_{13/2}$ at ϵ = 0.09 MeV, and the negative energy bound states $2f_{5/2}$ at ϵ = -1.73 MeV. The pairing gap energy of the resonant $1i_{13/2}$ state has a value $\Delta_{13/2} \approx 1.5$ MeV, which is close to that of bound states such as $1h_{9/2}$, $2f_{7/2}$ and $2f_{5/2}$, etc.

Another important aspect of the neutron rich nuclei is the formation of diffused neutron skin [1]. For the nucleus ^{156}Sn this characteristic feature is demonstrably seen in Fig. 5 wherein we plot the density distribution of protons for the nucleus ^{176}Sn by hatched area with the boundary marked by dashed line, and that of the neutrons for four different isotopes ^{100,132,156,176}Sn by solid lines. The tail of the neutron

density in the ^{156,176}Sn isotopes extends far beyond the mean field potential and has appreciable value up to about 15 fm. The proton densities are almost similar for different isotopes and we have shown only the results for the nucleus ^{176}Sn. The sharp fall off of the proton density distribution within a smaller distance as compared to that of neutron density is expected since the number of protons is small and the binding energy is large. A study of the neutron density profile reveals information about the nature of the surface thickness and diffuseness parameter. The surface thickness c is defined as the required change in radius to reduce $\rho(r)/\rho_0$ from 0.9 to 0.1 where ρ_0 is the maximum value of the neutron density. The diffuseness parameter α is determined by fitting the neutron density profiles to the Fermi distribution. It is found that with additional number of neutrons the surface thickness increases uniformly from about 1.75 fm in ^{100}Sn to about 3.4 fm in ^{176}Sn. Similar increase of about 90% is found for the diffuseness parameter α.

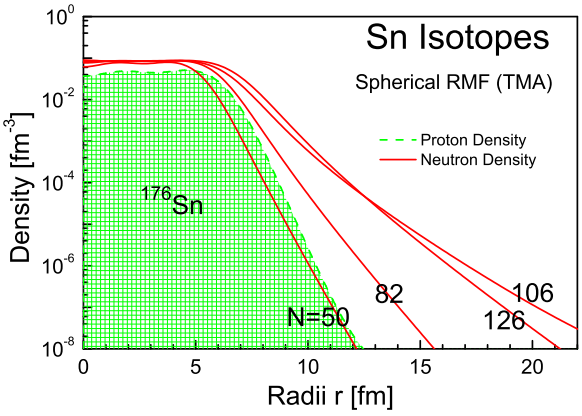

Fig. 5 – The neutron radial density distribution obtained for the ^{100,132,156,176}Sn isotopes have been shown by solid red coloured lines. The proton radial density distribution for the nucleus ^{176}Sn has been shown by hatched area marked with a dashed boundary.

The stability of such extremely neutron rich nuclei can be understood by studying the detailed single particle spectra and the variation of the Fermi energy with the addition of neutrons. Indeed it is found that the $1i_{13/2}$ state plays a crucial role in the sense that up to the neutron number N = 112, it adds to the binding through its contribution to the pairing energy by being a resonant state. Beyond the neutron number N = 112 this state becomes a bound one and contributes to the stability of neutron rich nucleus by accommodating more neutrons until it is completely filled at N = 126. Further addition of two neutrons fills the $4s_{1/2}$ level having energy 250 keV, which lies in the continuum. The total binding energy of the isotope ^{178}Sn is

less than that of ^{176}Sn by about 497 keV and thus the nucleus corresponding to N = 126 is suggested to be the heaviest bound isotope. It is found that the RMF theory yields a weaker spin orbit interaction with the addition of neutrons. Consequently the energy splitting between the spin-orbit partners, for example, $1h_{11/2}$ and $1h_{9/2}$ states, is gradually reduced from 8.2 MeV in ^{100}Sn to 5.7 MeV in ^{156}Sn, and gets further reduced to 4.95 MeV in ^{176}Sn as more and more neutrons are added to the system. Further, we observe that this change in the nature of the spin-orbit interaction for very rich neutron isotopes results in a negligible energy splitting of other high lying high angular momentum states. For example, the $1i_{11/2}$ and $1i_{13/2}$ spin-orbit partners usually have energy splitting of several MeV and this results in the neutron and proton magic numbers. In contrast for extremely neutron rich nuclei, for example in the case of ^{156,176}Sn nuclei this splitting is only about 2 to 4 MeV for these two states.

In contrast to the binding energy, the experimental data on the proton and neutron root mean square (rms) radii are available only for a few Sn isotopes [37,38]. The measured values for the proton rms radii [37] of $^{108-124}$Sn and that for the neutron rms radii [38] of ^{116,124}Sn isotopes are found to be in excellent agreement with our calculations as can be seen from Fig. 6. Our results once again are seen to compare well with that of the RHB calculations reported in ref. [20]. The RMF calculations predict a uniform increase of rms radii with the neutron number N. However, it does not follow exactly the $N^{1/3}$ systematics for the entire chain of isotopes. At the same time the calculations do not show any abrupt increase in the neutron rms radius as well. The neutron skin $\mathrm{r_n - r_p}$ increases from -0.07 fm for ^{100}Sn to 0.32 fm for ^{132}Sn, and then further to 0.76 fm for the ^{176}Sn isotope. For the neutron rich isotopes near the drip line the variation in neutron rms radius can be understood in terms of the occupancy of levels *viz.*, the $1i_{13/2}$ and $4s_{1/2}$ close to the Fermi surface. In contrast to the bound $1i_{13/2}$ state, the $4s_{1/2}$ state being in the continuum does not have appreciable localization inside the nucleus. Therefore, the contribution to the neutron rms radius from the $4s_{1/2}$ state is expected to be more than that from the $1i_{13/2}$ state assuming that both have the same occupancy.

For A> 156 the occupancy of the bound $1i_{13/2}$ state increases steadily as we add more neutrons. On the other hand the $4s_{1/2}$ state continues to be in the continuum just above the Fermi level and its very small occupancy does not change appreciably. This is the reason that we do not see pronounced rapid increase in the neutron rms radius and there is no obvious indication for the formation of neutron halo as we reach the neutron drip line.

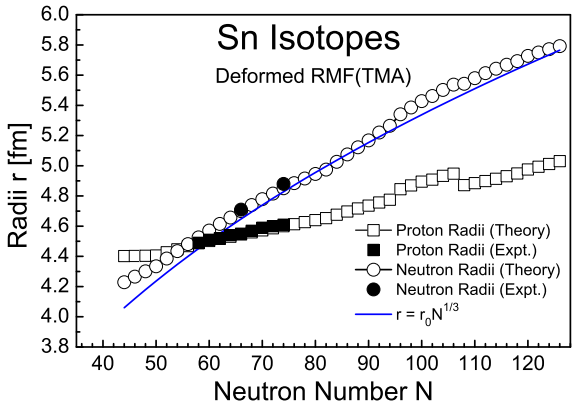

Fig. 6 – Calculated neutron and proton radii as a function of neutron number N for various Sn isotopes shown by open squares and circles, respectively, are compared with the available experimental data [37, 38] depicted by solid squares and circles, respectively. The blue solid line depicts a rough estimate for the neutron radius given by $r_n = r_0 N^{1/3}$ wherein the radius constant r_0 (= 1.15) is chosen to provide the best fit to the theoretical results.

4. CONCLUSION

Sn isotopes have been described in detail to elucidate the existence of extremely neutron rich nuclei with large |N - Z| values. We have investigated the role of single particle states lying close to the Fermi surface with regards to their contributions to the pairing energy, separation energy, rms radii and the related density profiles etc. in a detailed manner to understand the existence of extremely neutron rich isotopes of the Sn nucleus. It is found that the $1i_{13/2}$ state plays a crucial role in the sense that up to the neutron number N = 112, it adds to the binding through its contribution to the pairing energy by being a resonant state. Beyond the neutron number N = 112 this state becomes a bound one and contributes to the stability of neutron rich nucleus by accommodating more neutrons until it is completely filled at N = 126. It is also found that the RMF theory yields a weaker spin-orbit interaction with the addition of neutrons. Consequently the energy splitting between the spin-orbit partners, for example, $1h_{11/2}$ and $1h_{9/2}$ states, is gradually reduced from 8.2 MeV in ^{100}Sn to 5.7 MeV in ^{156}Sn, and gets further reduced to 4.95 MeV in ^{176}Sn as more and more neutrons are added to the system. Further, we observe that this change in the nature of the spin-orbit interaction for very rich neutron isotopes results in a negligible energy splitting of other high lying high angular momentum states. For example the $1i_{11/2}$ and $1i_{13/2}$ spin-orbit partners usually have energy splitting of several MeV and this results in the neutron and proton magic numbers. In contrast for extremely neutron

rich nuclei, for example in the case of ^{156,176}Sn this splitting is only about 2 to 4 MeV for these two states.

Two neutron drip line and two proton drip line are found to occur ^{176}Sn and ^{96}Sn respectively. The nucleus ^{94}Sn is found to satisfying the criteria and reported as a future candidate of two proton radioactivity. Results of RMF+BCS calculations for the two and one neutron separation energies are found to be in reasonably good agreement with the available experimental data [36].

Acknowledgements. Authors would like to express deep and sincere gratitude to Prof. H.L. Yadav, Banaras Hindu University, Varanasi, India for his guidance and constructive comments. The authors are indebted to Dr. L.S. Geng, RCNP, Osaka, Japan for valuable correspondence.

REFERENCES

1. I. Tanihata, J. Phys. **G 22**, 157 (1996).
2. Rituparna Kanungo, I. Tanihata and A. Ozawa, Phys. Lett. **B 512**, 261 (2001).
3. J. Dobaczewski, H. Flocard and J. Treiner, Nucl. Phys. **A 422**, 103 (1984).
4. J. Terasaki, P.H. Heenen, H. Flocard and P. Bonche, Nucl. Phys. **A 600**, 371 (1996).
5. K. Bennaceur, J. Dobaczewski and M. Ploszajczak, Phys. Lett. **B 496**, 154 (2000).
6. N. Sandulescu, R.J. Liotta and R. Wyss, Phys. Lett. **B 394**, 6 (1997).
7. M. Grasso, N. Sandulescu, Nguyen Van Giai and R.J. Liotta, Phys. Rev. **C 64**, 064321 (2001).
8. N. Sandulescu, Nguyen Van Giai and R.J. Liotta, Phys. Rev. **C 61**, 061301(R) (2000).
9. W. Nazarewicz *et al.*, Phys. Rev. **C53**, 740 (1996).
10. J.D. Walecka, Ann. Phys. (N.Y.) **83**, 491 (1974).
11. J. Boguta, A.R. Bodmer, Nucl. Phys. **A 292**, (1977) 413.
12. B.D. Serot and J.D. Walecka, Adv. Nucl. Phys. **16**, 1 (1986).
13. P.-G. Reinhard, M. Rufa, J. Marhun, W. Greiner and J. Friedrich, Z. Phys. **A 323**, 13 (1986).
14. Y.K. Gambhir *et al.*, Ann. Phys. (N.Y.) **198**, 132 (1990);
    P. Ring *et al.*, Comput. Phys. Commun. **105**, 77 (1997).
15. H. Toki, Y Sugahara, D. Hirata, B.V. Carlson and I. Tanihata, Nucl. Phys. **A 524**, 633 (1991).
16. Y. Sugahara and H. Toki, Nucl. Phys. **A 579**, 557 (1994).
17. P. Ring, Prog. Part. Nucl. Phys. **37**, 193 (1996).
18. M.M. Sharma, M.A. Nagarajan and P. Ring, Phys. Lett. **B 312**, 377 (1993).
19. J. Meng, P. Ring, Phys. Rev. Lett. **80**, 460 (1998).
20. G.A. Lalazissis, D. Vretenar and P. Ring, Phys. Rev. **C 57**, 2294 (1998).
21. M. Del Estal, M. Contelles, X. Vinas and S.K. Patra, Phys. Rev. **C 63**, 044321 (2001).
22. H.L. Yadav *et al.* Int. Jour. Mod. Phys. **E 13**, 647 (2004).
23. J. Meng, H. Toki, J.Y. Zeng, S.Q. Zhang and S.Q. Zhou, Phys. Rev. **C 65**, 041302(R) (2002).
24. G. Saxena *et al.*, Mod. Phys. Lett. **A 23**, 2589 (2008).
25. D. Singh *et al.*, Int. Jour. Mod. Phys. **E 21**, 1250076 (2012).
26. G. Saxena *et al.*, Int. Jour. Mod. Phys. **E 22**, 1350025 (2013).
27. J. Meng, I. Tanihata, and S. Yamaji, Phys. Lett. **B 419**, 1 (1998).
28. K. Sümmerer *et al.*, Nucl. Phys. **A 616**, 341 (1997).
29. K.L. Jones *et al.*, Nature **465**, 454 (2010).

30. C.B. Hinke *et al.*, Nature **486**, 341 (2012).
31. L.S. Geng *et al.*, Prog. Theor. Phys. **110**, 921 (2003);
L.S. Geng *et al.*, Prog. Theor. Phys. **113**, 785 (2005).
32. A.M. Lane, *Nuclear Theory* (Benjamin, 1964).
33. S.G. Zhou, J. Meng and P. Ring, Phys. Rev. **C 68**, 034323 (2003).
34. G.F. Bertsch, H. Esbensen, Ann. Phys. (N.Y.) **209**, 327 (1991).
35. A.B. Migdal, *Theory of Finite Fermi Systems and Applications to Atomic Nuclei* (Interscience, New York, 1967).
36. G. Audi, A.H. Wapstra, Nucl. Phys. **A 595**, 409 (1995).
37. H. de Vries, C.W. de Jager, C. de Vries, At. Data Nucl. Data Tables **36**, 495 (1987).
38. C.J. Batty, E. Friedman, H.J. Gils and H. Rebel, Adv. Nucl. Phys. **19**, 1 (1989).